Interpretation of magnetic data using boundary analysis and inversion techniques: a case study from Gölcük/Isparta (Turkey) region

Coşkun SARI* , **Emre TİMUR**
Engineering Faculty, Department of Geophysical Engineering, Dokuz Eylül University, İzmir, Turkey

Abstract: The Gölcük (Isparta) is on the southern side of the city of Isparta in the Mediterranean region of Turkey. The investigation of magnetic field strength variations over subterranean layers may reveal their locations on Earth's surface and provide physical and geometrical characteristics. Magnetic studies were carried out around Gölcük caldera lake using proton magnetometers to identify subsurface volcanic structures. The acquired data were inverted using four different edge detection algorithms such as analytic signal, tilt angle, theta map, horizontal gradient. Afterwards, the results were used to determine the locations of the anomalous structures. We also used pseudo-gravity and reduction-to-pole techniques for interpretation.

Additionally, the magnetic data were evaluated using the power spectrum technique and the results were compared with the 2D and 3D prismatic inversion outcomes. As a result, the boundaries and depth of the anomalous structures, such as the trachytic dome south of the Gölcük were determined for three different cross-sections and areas. The results show that the anomalous dome structures' average depth values vary between 225 m and 391 m in the region and the maximum depth of the Caldera reaches up to 1076 m.

Key words: Boundary analysis, Gölcük caldera, Isparta, inversion, power spectrum

1. Introduction

Geothermal energy is sustainable, reliable, cost-effective, and environmentally friendly but has been limited to areas near active tectonic plate boundaries. Recently, advances in technology have expanded the range of viable resources, particularly for applications such as greenhouse and home heating, opening a potential for widespread exploitation. Geothermal water production releases gases trapped deep within the Earth, however these emissions are much lower per energy unit than those of fossil fuel. Hence it became more important to detect new resource areas due to increasing population and growing industry. The critical element in the assessment, characterization and development of geothermal energy systems is to define the resource type and geometry (Moeck, 2014). Geophysical studies reveal valuable information about the location and depth of the three main elements of a geothermal system, the heater, the reservoir and the cap rock.

The study area is located in the west of the city of Isparta Province in SW Turkey. It is situated between the extending Western Anatolian Extensional Province and the Anatolian plateau which is relatively stable. The Isparta Angle can be defined as the main structural feature at the southwest part of Anatolia (Barka et al., 1995). It is located at the intersection of the Cyprus and Hellenic arc. The behavior of the area where Cyprus and the Hellenic arcs merge and interrelation with the

Isparta Angle structure is still not clear (Blumenthal, 1963; Glover and Robertson, 1998; Yagmurlu et al., 1997). Many geological and geophysical studies were performed since the 1970s to investigate mineralogy, petrography and industrial properties of the volcanic units outcropping around Isparta (Kalyoncuoglu et al., 2010; Platevoet et al., 2008, 2014; Schmitt et al., 2014; Dolmaz et al., 2018).

As a potential field method, magnetic measurements can be obtained from either the air or the ground covering a large scale and diverse purposes. Thus, the method has expanded from its initial use for finding and locating hematite ores to a more common method applied in the investigation for various minerals (Power et al., 2004), hydrocarbons[1], ground water (Smith and Pratt, 2003), archaeological ruins (Goussev et al., 2003; Timur, 2009; Tsokas and Papazachos, 1992), environmental contamination cases (Timur, 2014), landslide and seismic hazards (Finn et al., 2001; Langenheim et al., 2004), curie depth studies (Bilim, 2007), geothermal water resources and complex fault systems (Dolmaz, 2007; Goussev et al., 2004; Smith et al., 2002). The magnetic surveys can be used for mapping the surface geology precisely where the rocks carry magnetic minerals (Nabighian et al., 2005). Also an aeromagnetic investigation was carried out by Ekinci et al. (2020) in Mount Nemrut stratovolcano to determine the structural features of a caldera. The magnetic exploration which has been used for many years is one of the most useful

---

[1] Batchelor A, Gutmanis J (2002). Hydrocarbon production from fractured basement reservoirs-version7 [online]. Website www.geoscience.co.uk/downloads/fracturedbase mentver7.pdf [accessed 01 June 2020].

methods to identify buried structures such as geological formations including thermal water. This method is mostly influenced by ferromagnetic minerals, usually located along the geothermal areas' contact zones. Thus, the results obtained from an investigation of the magnetic field anomalies in such a seismically active area would contribute to a better understanding of the region's geological structure and tectonics.

In the present study, we collected total magnetic field intensity data to investigate the region's geological structure, using boundary analysis, power spectrum and inversion methods. Boundary analysis (edge detection) techniques are based on the position of maximum or zero points using horizontal or vertical derivatives, analytic signal amplitude, or their combinations (Wanyin et al., 2009). The findings obtained by using these techniques may be used as prior information which may guide inversion procedures (Sailhac and Gilbert, 2003). As effective commercial software packages and open-source codes have become widely available due to technological developments in computational procedures; thus edge-approximating techniques are being used more extensively (Salem et al., 2008; Balkaya et al., 2012; Ekinci et al., 2013). Moreover, the most important advantage is that the computation procedures do not require an assumption about the type of source body and the nature of the source. Our results are illustrated using several edge-approximation and boundary analysis techniques such as tilt angle, theta map, analytic signal, and horizontal gradient to define the boundaries very close to the city center of Isparta (Figure 1). Besides 2D-3D inversion and power spectrum methods were utilized to determine the geometry and depth of the bodies. We collected the data in 2015 using the equipment of Dokuz Eylül University and Dolmaz et al. (2018) also performed a geophysical study around the Gölcük caldera lake. We applied both 2D and 3D modelling techniques at three different locations and compared some of the the results with this study.

2. Geology of the Isparta-Gölcük region

Isparta region has attracted many earth scientists because of its complex geological features. There are many studies which were made to delineate the tectonic structures covering the study area (Yalçınlar, 1961; Poisson, 1977; Innocenti et al., 1982; Waldron, 1982; Poisson et al., 1984; Yalçınkaya et al., 1986; Karaman, 1990). The main geological formations in the area are Gölcük formation of Pliocene and its andesite members, Gönen conglomerates of Miocene, Erenler limestones of Cretaceous and Quaternary alluvium as the youngest formations (Figure 2).

The geological units can be classified into two main sections: allochthonous and autochthonous formations. Autochtonous units are generally Ağlasun Formation, Yazır Formation, Erenler Formation and Alluvium, where allochthonous units are Ophiolite Complex and Akdağ Formation. The Erenler limestone of the Cretaceous is the oldest rock of the autochthonous units in the study area. These limestones are overlain disconformably by Yazır formation of Aquitanian. The main lithology of this formation is reefal limestones. This formation is overlain conformably by Ağlasun Formation. Ağlasun Formation consists mainly of shale and sandstone of Burdigalian. Ophiolitic melange and Akdağ limestone units are thrusted tectonically onto Ağlasun formation in the Middle Miocene. The allochthonous rocks in this region are the Akdağ limestone units and the ophiolithic melange from Jurassic to Cretaceous. The youngest units of the study area are the Quaternary alluvium deposits. Between the Late Cretaceous and Early Paleocene periods, allochthonous rocks were emplaced in the region primarily. Quaternary alluvial deposits cover all these units. This tectonic feature can be defined as the most important event occured in the region, resulting in many faults and folds (Erdoğan, 2013).

The main tectonic structures such as overthrust or reverse faults and fold axes extend in the SE-NW direction, around the study area. Besides, the fracture systems and normal faults
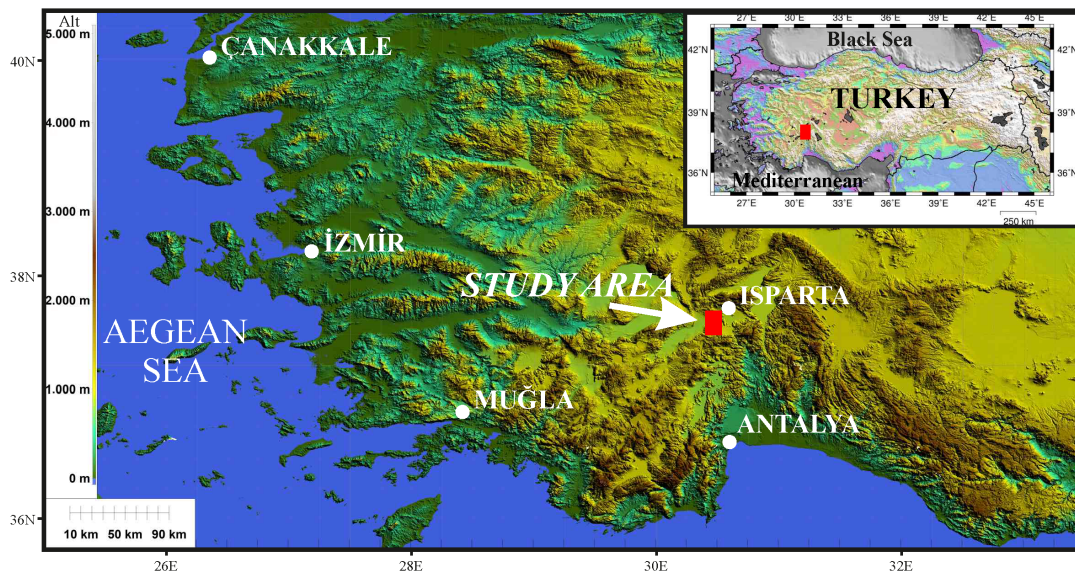

Figure 1. Location of the study area, indicated with red rectangle (not to scale).
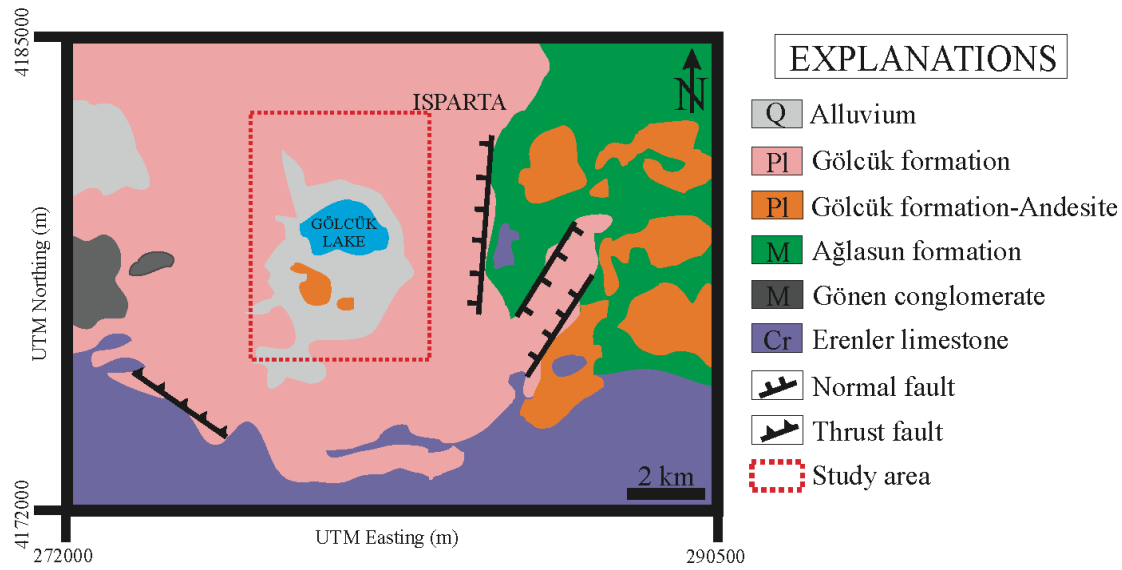
Figure 2. Geology of the study area (after Karaman, 1990; Yağmurlu et al., 1997).

are trending along the SW-NE direction. It is determined that all these geological structures have resulted under the SE-NW tensional forces and SW-NE compressional forces in this region.

Elitok et al. (2010) investigated that the present-day volcanic landforms just around the Gölcük caldera have been created by the last phreatoplinian eruptions of a maar-type volcanic activity, which ended with trachytic domes protruding within the maar crater. The crater edge mainly consists of remnants of tephriphonolitic lava flow-domes rimming the central depression occupied by the Gölcük caldera. Two recent intracaldera-like trachytic domes which are presented as Gölcük formation andesites in Figure 2, occupy the south-central part of the crater. According to the study of Platevoet et al. (2008), the thickness of the younger tuff rings are 75–80 m (from the altitude of 1600 m to 1520 m) and the thickness of main pyroclastic flow deposits are approximately 300 m (from the height of 1220 to 1520 m) in the region. They suggest small latite and trachyte domes and ancient protrusions in the NW of Gölcük caldera.

3. Data interpretation methods

3.1. Boundary analysis methods

The most important aim of interpreting magnetic field strength data is to identify the location and the geometry of magnetized sources. Recently, this aim has become significantly valuable as a result of expanding quantity of data collected for geothermal surveys. In order to obtain geometrical and physical magnetic source parameters, various mathematical methods based on the use of derivatives of the magnetic fields have been developed. In this study, the analytic signal, tilt angle, theta map, and the horizontal gradient methods were utilized. After this, the results of the techniques were compared.

3.1.1. Analytic signal

The analytic signal method for interpreting potential field data was introduced by Nabighian (1972). He showed that the

signal yields a bell-shaped function at the corners of a 2D polygonal structure. The maxima of the bell-shaped curves are located accurately over the corners, and half the width of the maximum amplitude of the curve is equal to twice the depth of the corner. As an advantage, the presence of remanent magnetization does not affect the determination of these parameters. It is possible to use this method to identify horizontal locations successfully, where the determination of depth is only reliable for 3D prismatic structures. The amplitude of an analytic signal obtained from 2D total magnetic intensity data, proposed by Roest et al. (1992), is commonly used in the interpretation of magnetic data for locating anomalies over their sources precisely. The equation of the analytic signal amplitude of a total magnetic field anomaly is expressed for prismatic structures as

$$A = \frac{\partial M}{\partial x}\hat{x} + \frac{\partial M}{\partial y}\hat{y} + i\frac{\partial M}{\partial z}\hat{z}, \qquad (1)$$

where M is the total magnetic field intensity, $\hat{x}$, $\hat{y}$ and $\hat{z}$ are unit vectors and i=$\sqrt{-1}$ (Roest et al., 1992). However, the direction of magnetization strongly affects the results, in conflict with the 2D cases (Nabighian et al., 2005).

3.1.2. Tilt angle

The enhanced local wavenumber (ELW) method is introduced by Salem et al. (2005) for interpretation of magnetic data collected along with the profiles. The amplitude of the tilt angle is similar to the local phase, calculated in the ELW method for evaluating magnetic field intensity. The sign of the horizontal gradient is used to obtain the local phase, whereas the tilt angle requires the horizontal gradient's absolute value. An automatic assessment of the location of a magnetized body can be obtained from the derivatives of the tilt angle from 2D magnetic data. The tilt angle can be defined as

$$\theta = tan^{-1}\left[\frac{\frac{\partial M}{\partial z}}{\frac{\partial M}{\partial h}}\right], \qquad (2)$$

where

$$\frac{\partial M}{\partial h} = \sqrt{\left(\frac{\partial M}{\partial x}\right)^2 + \left(\frac{\partial M}{\partial y}\right)^2} \qquad (3)$$

and $\partial M/\partial x$, $\partial M/\partial y$ and $\partial M/\partial z$ represent the partial derivatives of the magnetic field M in x, y and z directions.

3.1.3. Theta map

The theta angle map is a relatively new technique and it is used to process the magnetic contacts in a 2D total magnetic field intensity image. The method is mainly derived from the analytic signal and was defined before in Equation 1. For a vertical contact condition, $\partial M/\partial z=0$ and the signal vector makes an $\theta=0$ angle with the horizontal plane. If $\hat{s}$ is the unit vector of the analytic signal along the horizontal direction, the theta angle θ can be achieved as

$$\cos(\theta) = \frac{A \cdot \hat{s}}{|A||\hat{s}|} = \frac{\sqrt{(\partial M/\partial x)^2 + (\partial M/\partial y)^2}}{|A|} \qquad . \qquad (4)$$

Here $0 < \theta < \pi/2$ and Equation 4 define the ratio of the magnitude of the horizontal gradient and the amplitude of analytic signal. So that the theta map may also be thought of as a normalization of the horizontal gradient. The results are usually presented as well-defined images which are useful and convenient for direct interpretation (Wijns et al., 2005).

3.1.4. Horizontal gradient

It is possible to obtain the boundaries of the anomalous structure by calculating the maximum horizontal gradients of a magnetic field intensity anomaly map. In fact, if the edge is vertical and away from all other sources or edges, the maximum gradients are located exactly over the corners of the structure. The maximum horizontal gradients tend to locate over edges of potential field anomalies related to gravity or magnetic sources. The maximum gradients tend to define ridges over steep changes in density or magnetization in 2D surveys. Revealing the gradient's maxima can be done by simple inspection, however, by scanning the columns and rows of a gridded potential field data, an automated procedure records the locations of maximum horizontal gradients to a file for plotting and later analysis (Blakely, 1995).

Interpretation of the maximum horizontal gradients in terms of magnetization, density contrasts, and ultimately geology, involves some basic assumptions. Notably, the existing differences in physical properties should occur across abrupt and vertical edges or corners isolated from all other source bodies (Nabighian et al., 2005).

3.2. Pseudo-gravity and reduction to the pole

Pseudo-gravity is an interpretation method based on transforming of the total magnetic intensity anomalies into simpler gravity anomalies. The transformed anomalies are located in the vertical direction of the disturbing magnetized structures. So that the outcomes present eliminated distorsion due to the obliquity of the normal magnetic field (Baranov, 1957). The pseudo-gravity anomalies have all the usual properties of a gravity anomalies. The interpretation of pseudo-gravity maps becomes as easy as that of a Bouguer anomaly map and also they present no distortion. For performing the calculation of this transformation, firstly the magnetic intensity data should be collected on a trigonal or rectangular grid system, as for the usual calculation of the vertical derivatives. The gravitational potential U and the magnetic potential V and caused by a uniformly magnetized and uniformly dense body are related by a directional derivative, that is,

$$V = -\frac{C_m}{\gamma}\frac{M}{\rho}\hat{m} \cdot \nabla pU = -\frac{C_m}{\gamma}\frac{M}{\rho}g_m. \qquad (5)$$

It is possible to consider a variable distribution of density or magnetization to be composed of arbitrarily small regions of uniform density or magnetization; Equation (5) is suitable for each of the small regions and also invoking the superposition principle, should be appropriate for variable distributions of magnetization and density (Blakely, 1995). Further information can be found on Kanasewich and Agarwal (1970), Cordell and Taylor (1971), Bott and Igles (1972), Chandler and Malek (1991), Timur (2009) and Arısoy and Dikmen (2011).

A positive gravity anomaly tends to be located over a concentrated mass, but it is not the same for a magnetic anomaly when the ambient field and magnetization are not directed vertically. In general, if the magnetization and ambient field are not vertical, a symmetrical distribution of magnetization (such as a uniformly magnetized sphere) will produce a dipole anomaly rather than a symmetrical magnetic anomaly. Since the inclination and declination angle pair of the Earth's magnetic field is 57° and 4° in this region, the magnetic anomalies caused by magnetic bodies do not occur over the center of the sources. Due to this reason, the total field magnetic data first were transformed into the single magnetic pole, producing a reduced to pole (RTP) magnetic map where the highs are located more directly on their causative source and lows are suppressed or eliminated. The body magnetization direction was assumed to be equal to the Earth's magnetic field.

$$\mathcal{F}[\Delta T_t] = \mathcal{F}[\Delta T]\mathcal{F}[\varphi_t] \qquad (6)$$

$$\mathcal{F}[\varphi_t] = \frac{\theta_m^I \theta_f^I}{\theta_m \theta_f} \qquad (7)$$

We can use Equation (6), and then Equation (7) to transform a total field magnetic anomaly into the field's vertical component caused by the same source distribution magnetized in the vertical direction. The transformed anomaly in the Fourier domain is given by

$$\mathcal{F}[\Delta T_r] = \mathcal{F}[\varphi_r]\mathcal{F}[\Delta T]. \qquad (8)$$

The application of $\mathcal{F}[\varphi_r]$ is called reduction to the pole (Baranov and Naudy, 1964) because ΔT_r is the anomaly that is considered to be measured at the north magnetic pole, where ambient field and induced magnetization both would be directed down vertically (Blakely, 1995). Reduction to the pole removes one level of complexity from the interpretive process: It shifts anomalies laterally to be located over their causative sources and alters their shape so that symmetrical sources cause symmetrical anomalies.

3.3. 2D and 3D inversion methods

The magnetic data were interpreted using 2D inversion procedure. For this purpose, the LIMAT computer program written by Venkata Raju (2003) was used to obtain physical geometrical parameters of the buried structures for thick dike, thin sheet and fault models. The vertical fault and the thick dike models are consisted of thin sheets. Thus, for the fault and dike models, it is appropriate to use the similar initial

solution achieved for the thin-sheet model in the procedure. The initial solution is calculated automatically in this method by using the distances in terms of geometrical parameters and magnetic masurement values as inputs. Therefore, the obtained initial solution is modified by using Marquardt's (1963) nonlinear optimization technique, which employs an iterative procedure with nonlinear least squares regression. The regional value is adjusted in this method to achieve a close fit. The initial parameters with the models using the discrete magnetic anomaly values F(X) and the corresponding distances X may be obtained by rearranging the terms of

$$F(X) = P \frac{(X-D)sinQ + HcosQ}{(X-D)^2 + H^2} + MX + C, \quad (9)$$

where the equivalents of P and Q for the three components of magnetic field (vertical, horizontal and total) and other symbols are explained in Atchuta Rao et al. (1985) and Venkata Raju (2003). The purpose of inversion is to evaluate the unknown parameters P, D, Q, H, M and C of the body from a given distribution of F(X). Here, amplitude coefficient P and index parameter Q includes geometrical parameters of models like the angle of the profile with the magnetic north, inclination of the Earth's magnetic field, susceptibility contrast of the body to its surrounding, and inclination and declination of the resultant magnetization. Marquardt's (1963) method is used to avoid the singularity of G^TG and a constant known as Marquardt's parameter (λ) is added to the principal diagonal of G^TG which helps to control the eigenvalues so that they can not become zero. Modified Gauss–Newton solution can be written as

$$\Delta m = (G^T G + \lambda I)^{-1} G^T \Delta F, \quad (10)$$

where m represents model parameters, G is the Jacobian matrix of partial derivatives of F(X) and ΔF includes measured values. The inversion method depends on the choice of λ. Initially, a large positive value is given as an input to the computer program. If the RMS error is reduced, λ is divided by a constant factor (4 in the present study) and reduced. If the RMS error is increased during the iterations, λ is increased by multiplying it by a constant (2 in the present study) until convergence resumes. Background level of the magnetic field intensity is 45650 nT in the study area. The profile azimuths were 45º for A-A' and C-C' profiles and 0º for B-B'.

We used vertical 3D models which are widely used prismatic geometries for interpreting magnetic anomalies. Bhattacharya (1964) proposed an equation for calculating the total field magnetic anomalies of a 3D model. In general, it is hard to separate the anomalies resulting from individual prisms, in case of the magnetized bodies are close to each other. Additionally, Bhattacharya (1980) developed a new method for solving the normal equations using Cholesky decomposition. The trigonometric and logarithmic terms are simplified by Kunaratram (1981) in the anomaly equation using complex notations. Rao and Babu (1993) presented an effective 3D interpretation technique using approximate equations for rapid calculation of anomalies and their derivatives. The approximate anomaly equation is presented, which treats the prism as a line mass (Rao and Babu, 1993).

$$\Delta T (x,y,0) = A \left[\begin{array}{c} (G_1\beta + G_2\alpha)\left(\frac{1}{R_1^3} - \frac{1}{R_2^3}\right) + \frac{G_3 C_1 \alpha \beta}{(\alpha^2 + \beta^2)} \\ - \frac{G_4(C_1\beta^2 + C_2)}{(\alpha^2 + \beta^2)} - \frac{G_5(C_1\alpha^2 + C_2)}{(\alpha^2 + \beta^2)} \end{array} \right] \quad (11)$$

where $G_{1,2,3,4,5}$ are physical, $A, \alpha, \beta, R_1, R_2, C_1$ and C_2 are geometrical parameters. Subroutines one_prism.m and multi_prism.m from Mendonça and Meguid (2008) were used to compute 3D magnetic anomalies. Arısoy and Ulugergerli (2005) and Timur (2009; 2017) investigated different receiver separations and orientations for the magnetic gradiometer surveys used to investigate near-surface structures. Abedi et al. (2015), Wang et al. (2015) and Utsugi (2019) studied similar 3D inversion techniques using prismatic bodies. The 3D prismatic model for total magnetic field anomaly is presented in Figure 3.

3.4. Power spectrum method

The word spectrum is generally used to describe the variation of certain quantities such as amplitude or energy as a function of parameters, normally wavelength or frequency. We may obtain a frequency spectrum when a signal is expressed as a function of frequency. Mathematically, $f(t)$ as a time-domain signal, can be expressed by $F(w)$, where w represents angular frequency ($w = 2\pi f$; f is the linear frequency). The $F(w)$ is generally a complex function and can be represented by the sum of the real and imaginary parts $F(w) = a(w) + ib(w)$. Where $|F(w)|$, the amplitude spectrum is defined as

$$|F(w)| = \sqrt{a^2(w) + b^2(w)}. \quad (12)$$

If E is the power of a real function, $f(t)$ with a period of T can be expressed as

$$E = lim_{T\to\infty} \frac{1}{2T} \int_{-T}^{T} (f(t))^2 dt. \quad (13)$$

Here $(f(t))^2$ term is instantaneous energy and this integration gives the total energy of the function. According to Parseval's theorem (Thompson, 1982) the power spectrum $|F(w)|^2$ and the total energy E_T are related by

$$E_T = \frac{1}{2\pi} \int_{-\infty}^{\infty} |F(w)|^2 dw = \frac{1}{\pi} \int_{0}^{\infty} |F(w)|^2 dw, \quad (14)$$

where the power spectrum $|F(w)|^2$ is a real quantity. The power spectrum method can be applied to potential field data and mainly used for estimating the average depth to the source body, such as a basement rock or the thickness of the sedimentary layers (Blakely, 1995). Detailed information about the power spectrum method is proposed by Spector and Grant (1970). The method was applied to the three cross-sections' magnetic data at various directions over the anomalies.

4. Magnetic studies and results

Magnetic measurements were carried out around Gölcük caldera, to estimate the depths of the anomalous geological structures. We collected the grid data at every 50 m in X and Y direction, along 96 profiles and used Scintrex ENVI/MAG Proton magnetometer with a sensitivity of ±0.1 nT which is adequate for such an investigation. A second proton magnetometer (Geometrix G-856) monitored the diurnal variation at a base station during the survey and the measurements were also subtracted from the observed magnetic data to remove the effects of the possible abrupt

changes of the Earth's magnetic field from the data (Figure 4). The studies cover the area between volcanic Gölcük caldera and Ağlasun district along the Isparta-Antalya highway in the south. Dolmaz (2007; 2016) and Dolmaz et al. (2018) performed previous regional magnetic investigations around the study area and aimed to reveal the effect of Fethiye Burdur Fault Zone (FBFZ).

The high-resolution mode is selected on the equipment for measurements and the RMS value of the data was less than 0.1. The collected spatial data were gridded and the total magnetic field intensity map is presented in Figure 5. We

performed several boundary analysis techniques such as the analytic signal, tilt angle, theta map and horizontal gradient methods. The analytic signal map was prepared for detecting the location of the subsurface anomalous structures. Yellow and red color high amplitude anomalies indicate possible anomalous bodies in the south and NW of the study area (Figure 6). The high amplitude anomaly represents the intracaldera-like trachytic dome located in the south of Gölcük. Another high anomaly was noticed extending NE-
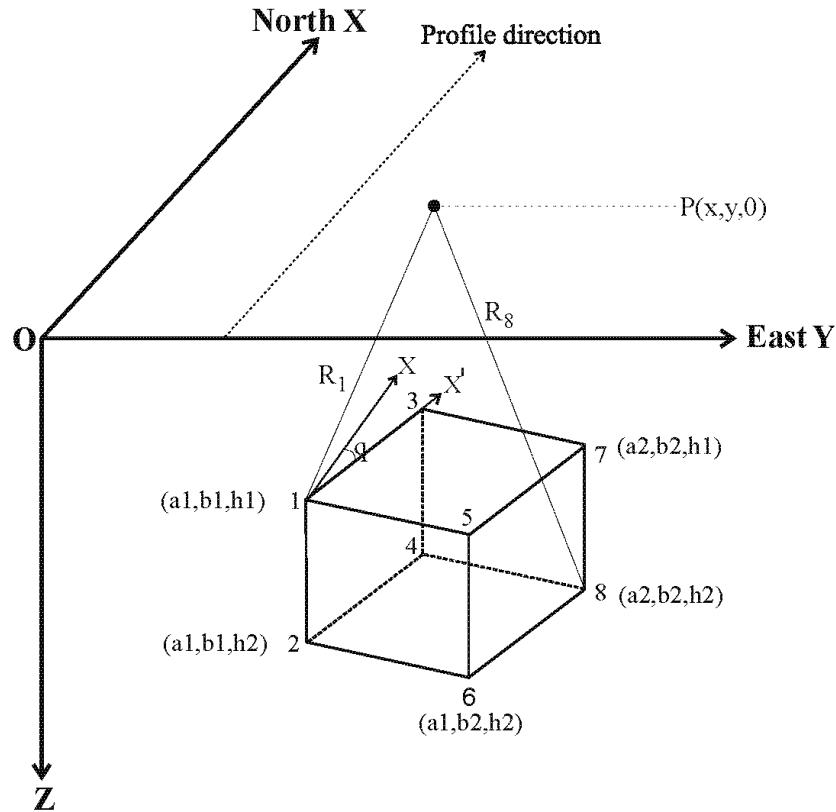

Figure 3. 3D rectangular prism model (after Timur, 2017).

Figure 4. Pictures from the magnetic survey. Base station on the left and mobile measurement station on the right.
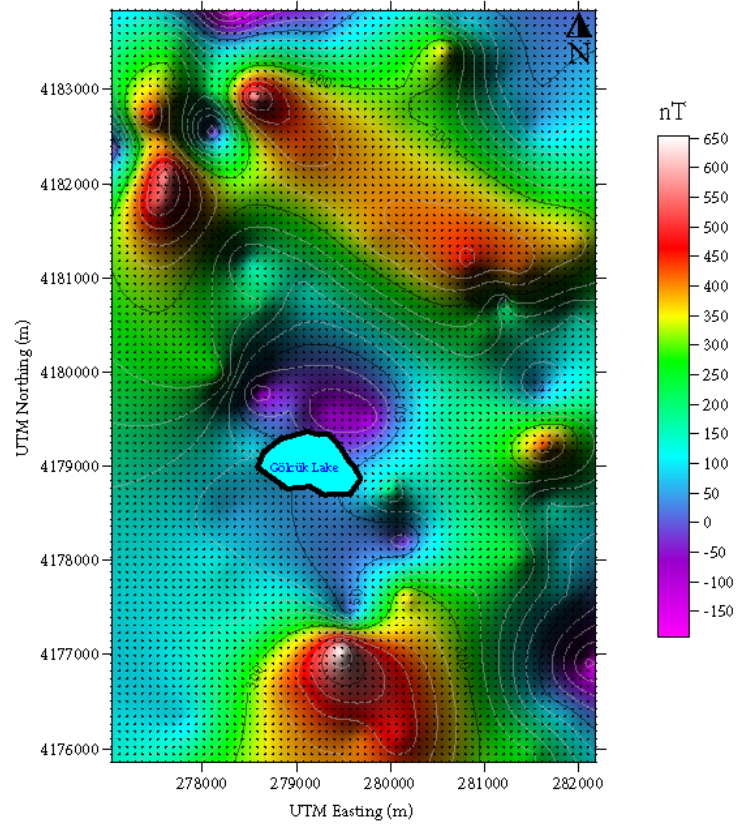
Figure 5. Total magnetic field anomaly map. Black points indicate the measurement stations.
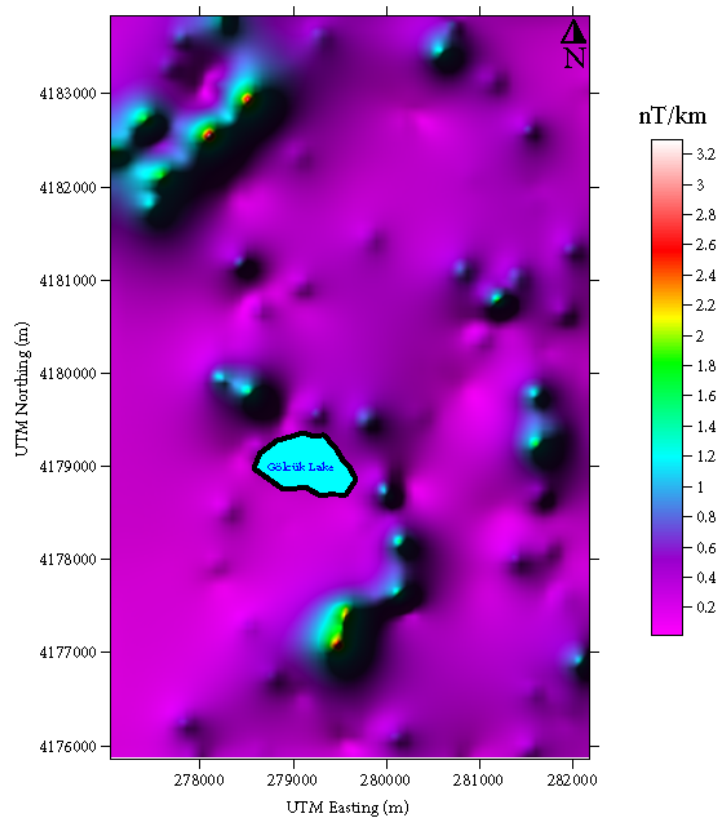

Figure 6. Analytic signal map of the magnetic anomaly.

SW direction in the northeast of the map is considered to be the effect of small latite and trachyte domes and ancient protrusions. A tilt angle map is also prepared for delineating the borders of possible structures. High amplitude red color anomalies indicate the volcanic structures in the NW and south of the Caldera (Figure 7), located almost in the center of the study area. Also, high-value anomalies in the NE of the study area support the analytic signal map of the area. The study area's theta map presents the opposite amplitudes of the tilt angle map (Figure 8). Low amplitude anomalies cover the volcanic lake area. Both tilt angle and theta map results support the existence of covered volcanic bodies but they also present many other low-amplitude anomalies. Moreover, the horizontal gradient method was applied to data, and the maximum amplitude values were plotted over the magnetic anomaly map (Figure 9). The maximum amplitude differences are indicated with different symbols and the distribution of the gradient values also support the existence of anomalous structure around the Caldera and also South and NW of the study area. The pseudo-gravity map of the area presents two high amplitude positive gravity anomalies in the south and NW of the area (Figure 10). Furthermore it is possible to see the effect of the Caldera at the center of the study area as a low amplitude purple color anomaly. Considering the geological study of Platevoet et al. (2008), the covered latite and trachyte domes present wider high amplitude anomalies in the north and NW of the study area.

The power spectrum method was used to obtain the average depths of the anomalous structures. For this purpose, three different cross-sections (Figure 11) were calculated from magnetic anomaly map (Figures 12a–12c). Locations of the A-A' and B-B' sections were selected to define the anomalous structures around the Caldera. Also C-C' section is chosen as a result of the high and low amplitude anomalies in the NW of the study area where the covered latite and trachyte domes exist. The structural depths to the near-surface units (Alluvium and younger tuff rings) were calculated to be 46 m, 43 m and 25 m, respectively. The depths of the structures representing the topography of the basement units (Limestones and Ağlasun formation volcanics) in the same areas we found to be 1002 m, 380 m and 225 m (Figures 13a–13c).

After calculating the average depths from the power spectrum method, 2D inversion was carried out for the same (A-A', B-B' and C-C') profiles, to achieve other geometrical and other physical parameters. The red dots indicate the cross-section data, blue lines indicate the calculated data for thin sheet models, the green lines indicate the calculated data for dike models and the yellow lines indicate the calculated data for fault models (Figures 14a–14c). We used the anomaly parts, which represent the structure precisely. The calculated physical and geometrical parameters, inversion numbers and RMS errors are presented in Tables 1–3.

The calculated depths from the power spectrum and 2D inversion methods are following the depths defined by Karaman (1990) for the Gölcük and Ağlasun formation volcanics. The Gölcük caldera shows a low magnetic anomaly, however, the Andesites in the South of the Lake show high
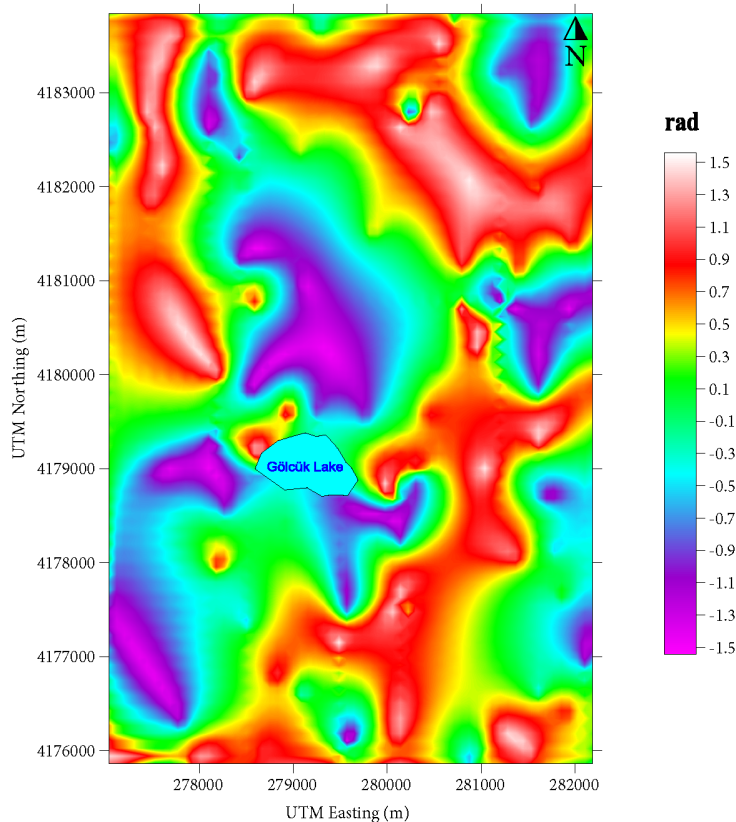

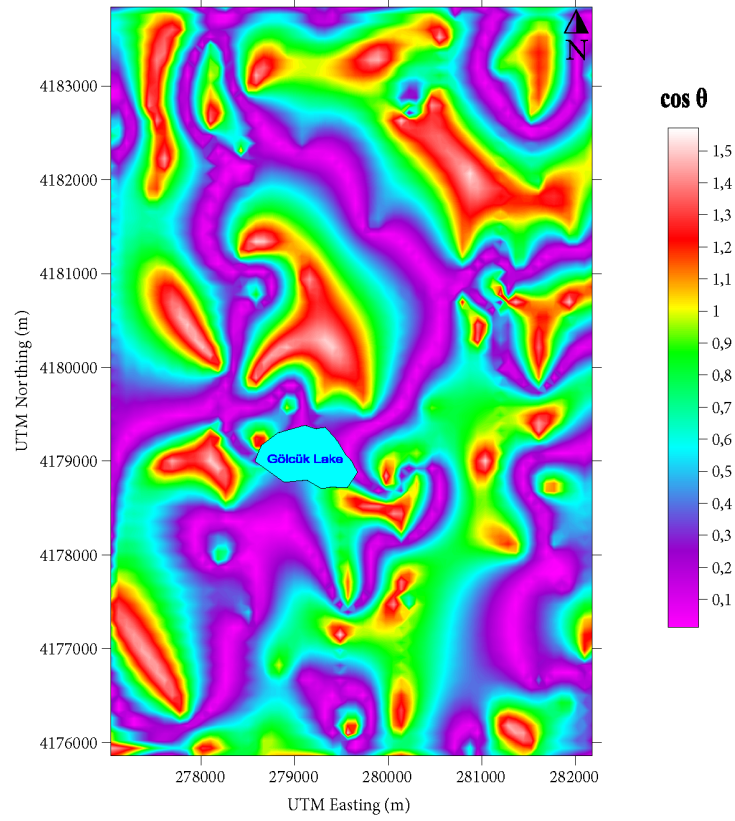**Figure 7.** Tilt angle map of the magnetic anomaly.
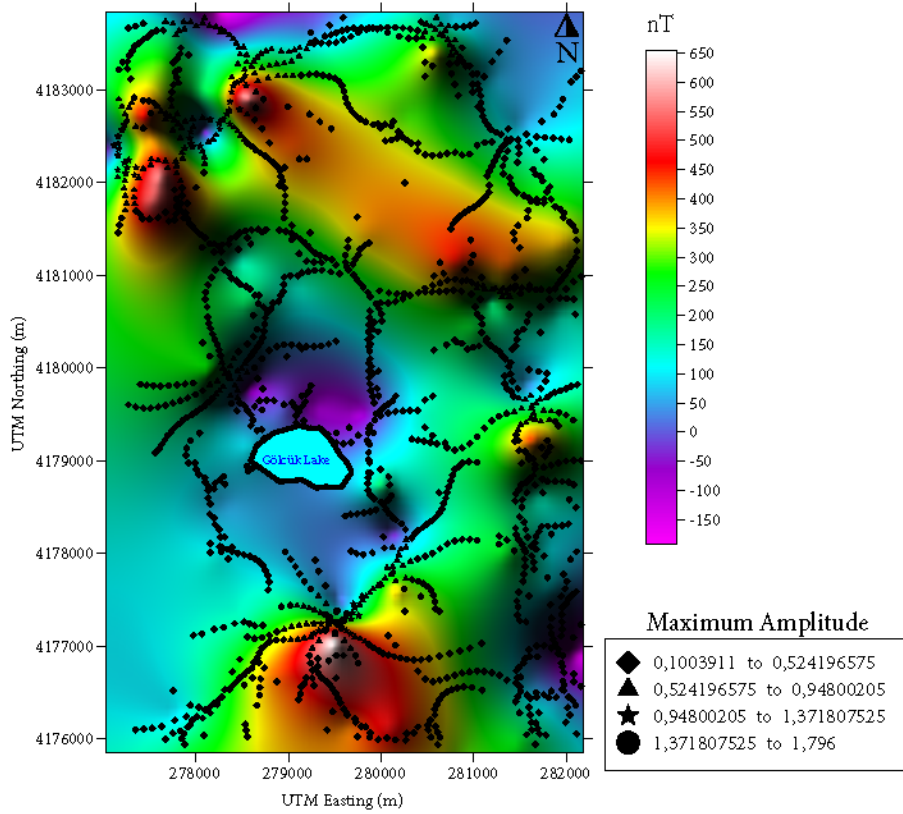
Figure 8. Theta map of the magnetic anomaly.

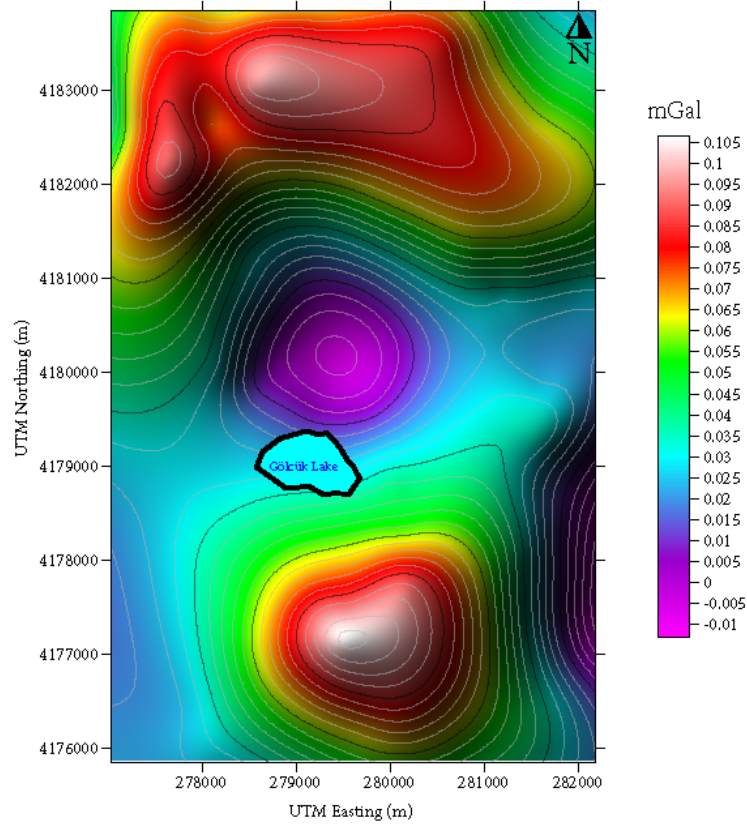**Figure 9.** Horizontal gradient values and magnetic anomaly map.

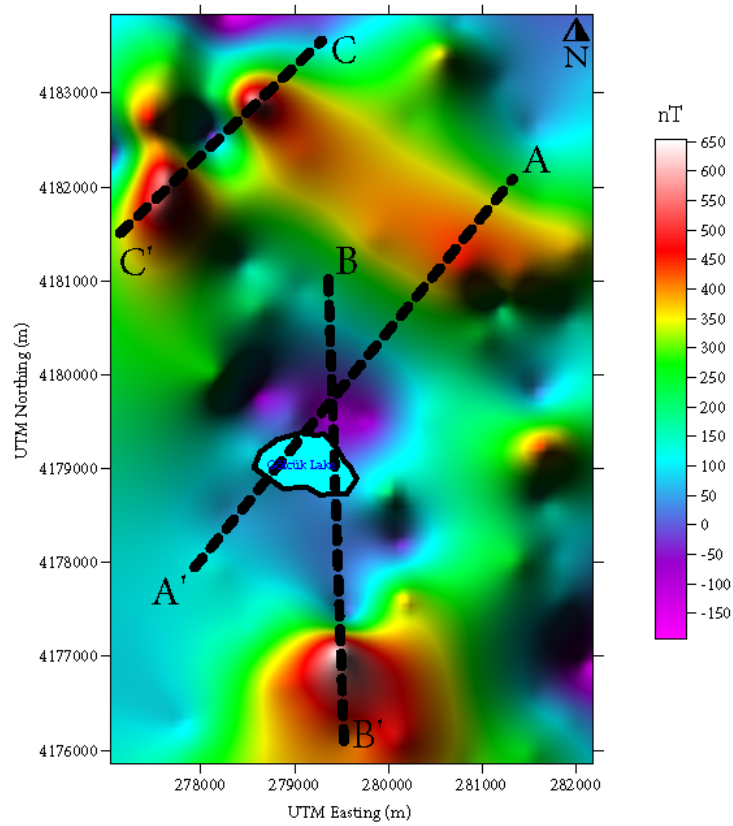**Figure 10.** Pseudo-gravity map of the study area.

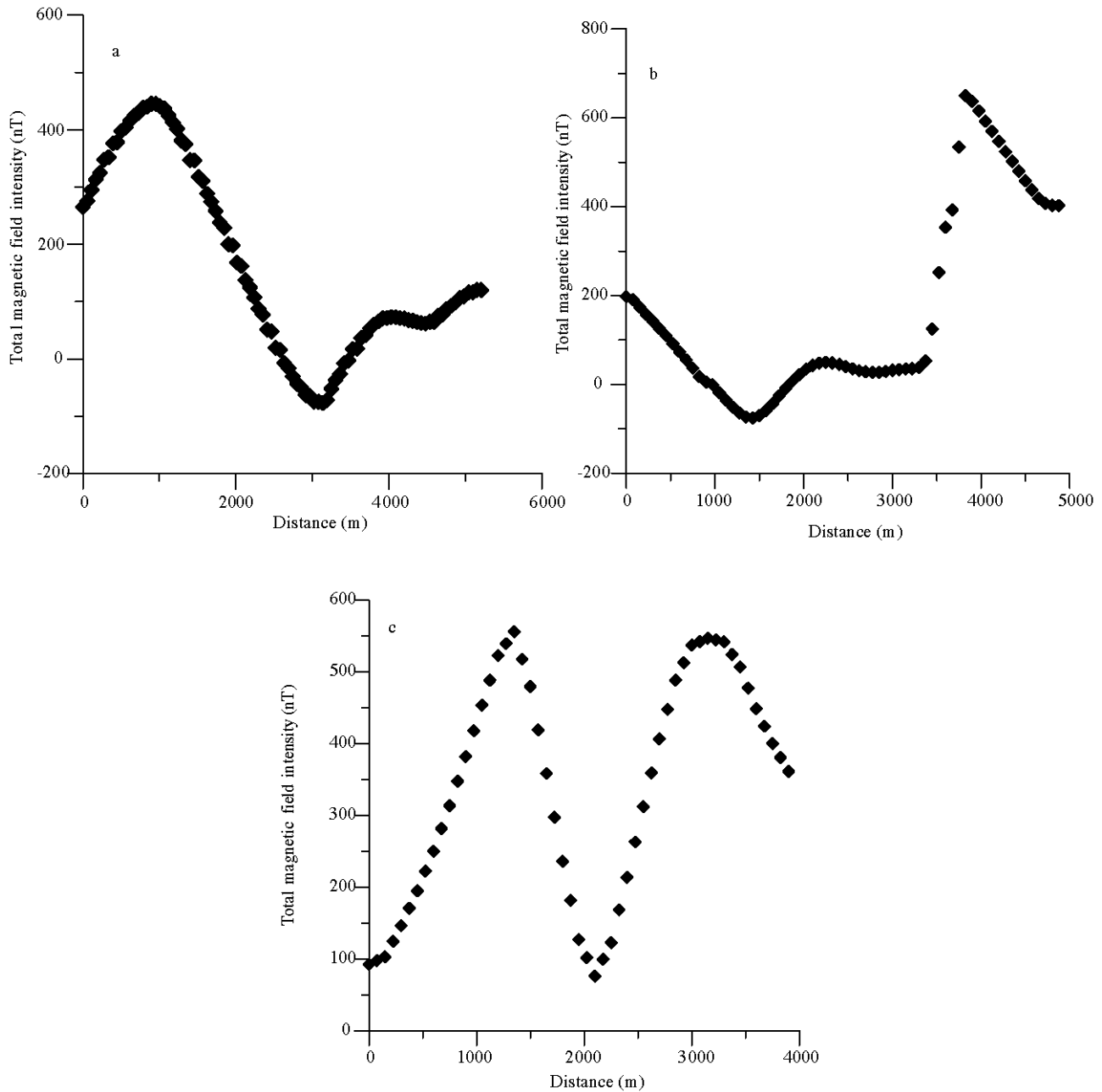**Figure 11.** Locations and directions of three cross-sections.

Figure 12(a). Anomaly of A-A' cross-section, **(b):** Anomaly of B-B' cross-section, **(c):** Anomaly of C-C' cross-section.

magnetic anomalies. The depth of the structure calculated from the A-A' section is around 1100 m for thin sheet and dike models, where it is calculated as 1002 m from the power spectrum. It is clear that the anomalous structure is deeper around the Caldera than the surrounding area. The depth values calculated for B-B' section are 356 m, 340 m and 343 m for thin sheet, dike and fault models and 380 m for power spectrum. The location of B-B' section intersects with the contact of Gölcük formation andesites and alluvium. The outcrop of the volcanic members of the Gölcük formation indicates and supports a shallow magnetic anomalous structure in the area. The location and direction of C-C' section are selected due to the anomalies observed in the boundary analysis methods, pseudo-gravity map, and

geological data proposed by Platevoet et al. (2008). The calculated depth from 2D inversion (230–294 m) and the power spectrum (225 m) support a shallow magnetic anomalous structure in the NW of the Caldera.

We considered three prismatic models for interpreting the anomalous structures in the study area. The first model is located at the NW of the area, where high amplitude magnetic anomalies exist. The location of the second model is selected in the north of the Gölcük caldera and the third model is selected at the south of the Caldera where the highest amplitude anomalies were observed. The magnetic anomaly map converted to the reduced-to-the-pole anomaly map before performing the 3D inversion (Figure 15). The horizontal initial geometrical model parameters are selected
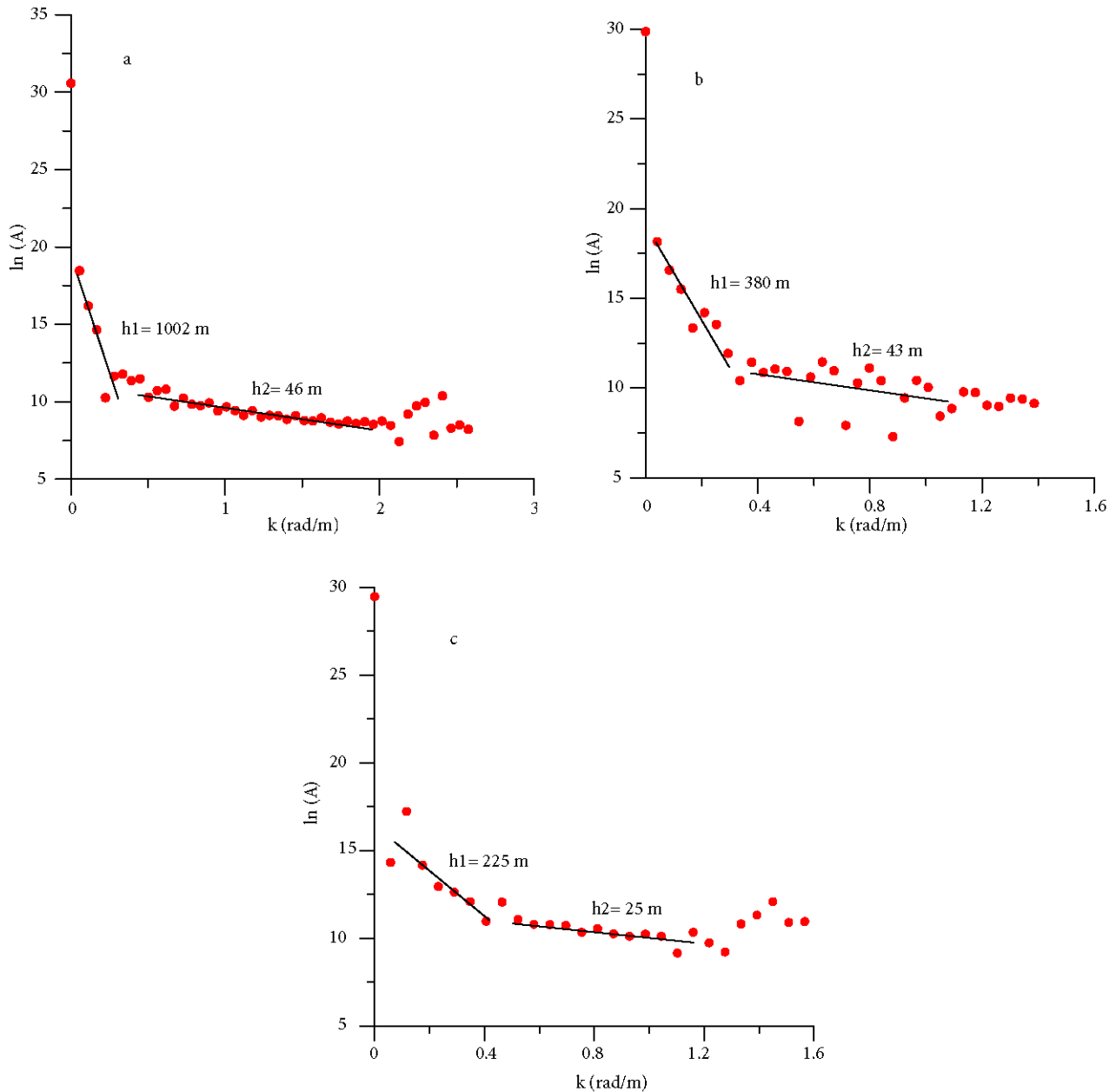
Figure 13(a). Power spectrum and calculated depths of A-A' cross-section, **(b):** Power spectrum and calculated depths of B-B' cross-section, **(c):** Power spectrum and calculated depths of C-C' cross-section.

according to the results of boundary analysis and pseudo-gravity transformation, where vertical geometrical initial parameters are chosen due to the results of the power spectrum and 2D inversion. After performing inversion, we achieved 281 m, 986 m and 391 m as top depths for 3D models 1, 2, and 3, respectively (Table 4). Dolmaz et al. (2018) calculated the top depth as 400 m for the location of model 3. The calculation of inversion took maximum 18 iterations for all models to reach an RMS error value of <0.01. These depth values are in accordance with the values achieved with power spectrum and 2D inversion results, especially for thin sheet and dike models.

5. Discussion and conclusion
Gölcük caldera is geologically one of the most important and young volcanic sites in the Aegean Region. This volcanic activity took place at the apex of the Isparta Angle at the intersection of Lycian and Antalya nappes. Firstly, we carried out magnetic measurements, then boundary analysis, power spectrum and inversion methods in this area respectively. The boundary analysis methods supported precious information about the location and geometry of the structures and therefore the locations and directions of the cross-sections were selected quickly and precisely. We obtained useful results from analytic signal amplitude and horizontal gradient maps, where relatively more complex outcomes from tilt
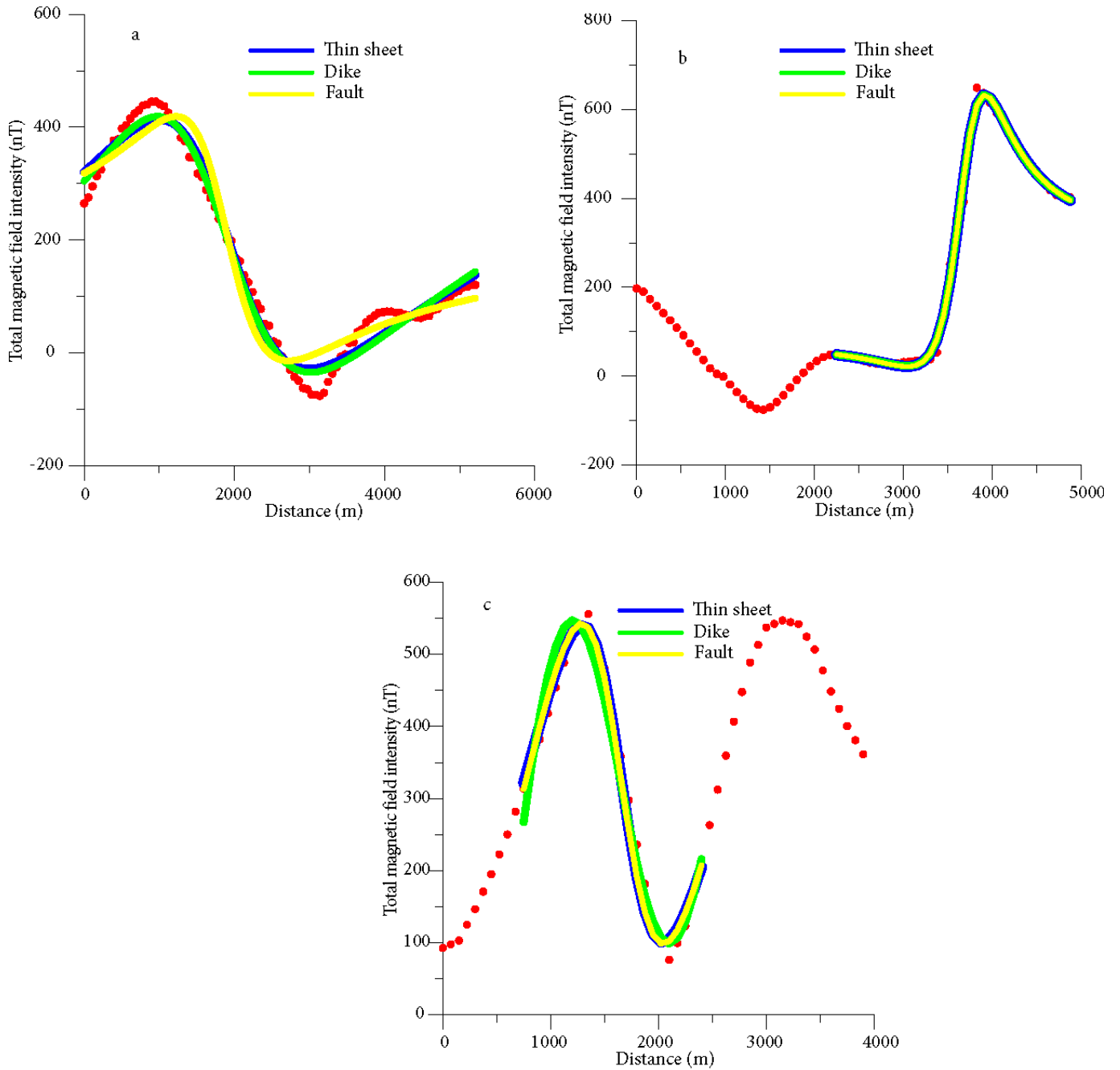
Figure 14. Measured and calculated 2D inversion results. The red dots indicate the measured data; blue, green and yellow lines represent the calculated data for thin sheet, dike and fault models, **(a):** A-A' cross-section, **(b):** B-B' cross-section, **(c):** C-C' cross-section.

Table 1. Calculated parameters from 2D inversion for thin sheet model.

Thin sheet model	A-A' cross-section	B-B' cross-section	C-C' cross-section
Top depth (m)	1172.3	356.4	294.56
Distance to origin (m)	1848.4	1445.2	643
Width (m)	117.3	35.65	39.46
RMS error	0.319	0.052	0.12
Iteration number	38	14	39

Table 2. Calculated parameters from 2D inversion for thin dike model.

Dike model	A-A' cross-section	B-B' cross-section	C-C' cross-section
Top depth (m)	1076.05	340.13	290.81
Distance to origin (m)	1765.37	1445.09	643.02
Width (m)	530.6	96.58	39.46
RMS error	0.423	0.052	0.1274
Iteration number	39	42	41

Table 3. Calculated parameters from 2D inversion for fault model.

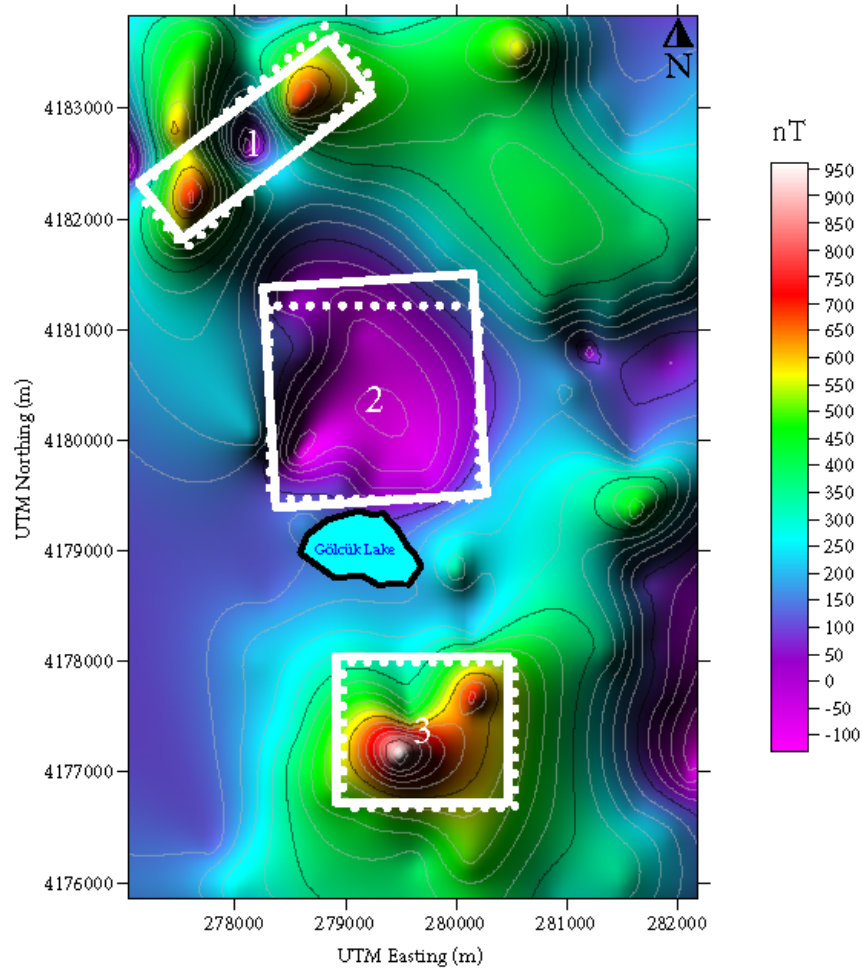| Fault model	A-A' cross-section	B-B' cross-section	C-C' cross-section
Top depth (m)	737.40	343.14	293.62
Distance to origin (m)	1856.39	1444.01	641.17
Bottom depth (m)	769.24	373.63	435.92
RMS error	0.659	0.052	0.1249
Iteration number	38	41	41

Figure 15. Initial (white dash line) and interpreted (white line) models overlaid on reduced to the pole magnetic anomaly map.

Table 4. Initial and interpreted 3D model parameters for three prismatic bodies (RMS < 0.01).

Prism No	Model	a_1 (m)	a_2 (m)	b_1 (m)	b_2 (m)	h_1 (m)	h_2 (m)	I_O (Deg)	D_O (Deg)	Θ (Deg)	EI (CGS)
1	Initial model	350	1750	5900	7800	250	300	57	4	42	0.006
	Interpreted model	346	1758.6	5871.3	7786.2	**281.2**	**336.7**	54.6	4	39.9	0.0091
2	Initial model	1200	3100	3500	5200	1000	1100	57	4	0	0.006
	Interpreted model	1210.3	3134.8	3453.1	5176.9	**986.2**	**1046.6**	55.1	3.8	0.6	0.0042
3	Initial model	1900	3400	850	2000	350	450	57	4	0	0.006
	Interpreted model	1872.5	3352	871.9	2042	**391.3**	**453.2**	56.8	4.1	0.1	0.01

angle and theta maps. After performing boundary analysis methods, we considered that there are three main anomalous structures in the study area and calculated the depths and other geometrical parameters using power spectrum, 2D and 3D inversion procedures. The thickness of the near-surface structures (alluvium formations and tuff) were found to be 25 m, 43 m, and 46 m for the area and these results are consistent with the previous geological studies. Firstly, a high anomaly is observed and located to the NW of the study area where ancient protrusions exist. Previous geological studies propose small latite and trachyte domes and ancient protrusions that can not be identified from the surface in the NW of the study area. Our study revealed the existence and location of these subsurface structures that have a varying depth of between 225 m and 294 m. Secondly, a low anomaly located to the north of Gölcük Lake is selected for modeling. After performing the modeling procedures, we achieved that the depth of the anomalous structure varies between 986 m and 1076 m. We believe that the thickness of the main pyroclastic flow deposits is very high here, however, this area needs to be investigated in detail to determine the structure of the caldera

and the reason beneath this low anomaly. Thirdly, a high anomaly located to the south of Gölcük Lake is modelled. Here depth is found to be between 340 and 391 m. Other researchers investigated this area and the depth was calculated as 400 m. Thickness and depths of this trachytic dome achieved in our study and previous studies are in consistent. We performed similar numerical results with power spectrum, 3D inversion and especially dike model in 2D inversion.

References

Abedi M, Siahkoohi H, Gholami A, Norouzi G (2015). 3D inversion of magnetic data through wavelet based regularization method. International Journal of Minining and Geophysical Engineering 49: 1-18. doi: 10.22059/ijmge.2015.54360

Arısoy MO, Ulugergerli EU (2005). Evaluation of different receiver orientations and receiver separations in magnetic gradiometer method. Journal of the Balkan Geophysical Society 8: 229-232.

Arısoy MO, Dikmen Ü (2011). Potensoft: MATLAB-based software for potential field data processing, modeling and mapping. Computers and Geosciences 37: 935-942.

Balkaya Ç, Göktürkler G, Erhan Z, Ekinci YL (2012). Exploration for a cave by magnetic and electrical resistivity surveys: Ayvacık sinkhole example, Bozdağ İzmir (western Turkey). Geophysics 77 (3): B135-B146.

Baranov V (1957). A new method for interpretation of aeromagnetic maps: pseudo-gravimetric anomalies. Geophysics 22: 359-383.

Baranov V, Naudy H (1964). Numerical calculation of the formula of reduction to the magnetic pole. Geophysics 29: 67-79.

Barka A, Reilinger R, Saroğlu F, Şengör AMC (1995). The Isparta Angle: its evolution and importance in the tectonics of the eastern Mediterranean region. In: International Earth Science Colloquium on the Aegean Region; Izmir, Turkey. p. 6.

Bhattacharya BK (1964). Magnetic anomalies due to prism shaped bodies with arbitrary polarization. Geophysics 29: 517-531. doi: 10.1190/1.1439386

Bhattacharya BK (1980). A generalized multibody for ınversion of magnetic anomalies. Geophysics 45: 255-270. doi: 10.1190/1.1441081

Bilim F (2007). Investigations into the tectonic lineaments and thermal structure of Kutahya Denizli region, western Anatolia, from using aeromagnetic, gravity and seismological data. Physics of the Earth and Planetary Interiors 165 (3-4): 135-146.

Blakely RJ (1995). Potential Theory in Gravity and Magnetic Applications. Cambridge, UK: Cambridge University Press.

Blumenthal M (1963). Le systeme structural du Taurus sud-Anatolien, In Livre a'memoire du Professeur P. Fallot. Mémoires de la Société géologique de France 2: 611-662.

Bott MHP, Ingles A (1972). Matrix methods for joint interpretation of two-dimensional gravity and magnetic anomalies with application to the Iceland-Faeroe Ridge. Geophysical Journal of the Royal Astronomical Society 30: 55-67.

Chandler VW, Malek KC (1991). Moving-window Poisson analysis of gravity and magnetic data from the Penokean orogen, east-central Minnesota. Geophysics 56: 123-132.

Cordell L, Taylor PT (1971). Investigation of magnetization and density of a North Atlantic seamount using Poisson's theorem. Geophysics 36: 919-937.

Dolmaz MN (2007). An aspect of the subsurface structure of the Burdur-Isparta area, SW Anatolia, based on gravity and aeromagnetic data, and some tectonic implications. Earth Planets Space 59: 5-12.

Dolmaz MN (2016). Depth Estimation From the Magnetic Anomalies of the Northern end of the Fethiye-Burdur Fault Zone (FBFZ), SW Turkey. In: International Conference on Engineering and Natural Sciences; Sarajevo, Bosnia. pp. 1873-1876.

Dolmaz MN, Oksum E, Erbek E, Tutunsatar HE, Elitok O (2018). The nature and origin of magnetic anomalies over the Gölcük caldera, Isparta, South-Western Turkey. Geofizicheskii Zhurnal 3 (40): 145-156.

Ekinci YL, Büyüksaraç A, Bektas O, Ertekin C (2020). Geophysical investigation of Mount Nemrut stratovolcano (Bitlis, Eastern Turkey) through aeromagnetic anomaly analyses. Pure and Applied Geophysics 177 (7): 3243-3264. doi: 10.1007/s00024-020-02432-0

Ekinci YL, Ertekin C, Yiğitbaş E (2013). On the effectiveness of directional derivative based filters on gravity anomalies for source edge approximation: synthetic simulations and a case study from the Aegean graben system (western Anatolia, Turkey). Journal of Geophysics and Engineering 10: 1-15. doi: 10.1088/1742-2132/10/3/035005

Elitok Ö, Özgür N, Drüppel K, Dilek Y, Platevoet B et al. (2010). Origin and geodynamic evolution of late Cenozoic potassium-rich volcanism in the Isparta area, southwestern Turkey. International Geology Review 52 (4-6): 454-504.

Erdoğan M (2013). Hydrogeological investigation of Burdur-Ağlasun Basin. MSc Thesis, İstanbul Technical University, İstanbul, Turkey.

Finn CA, Sisson TW, Deszcz-Pan M (2001). Aerogeophysical measurements of collapse-prone hydrothermally altered zones at Mount Rainier Volcano. Nature 409: 600-603.

Glover C, Robertson A (1998). Neotectonic intersection of the Aegean and Cyprus tectonic arcs: extensional and strike-slip faulting in the Isparta Angle, SW Turkey. Tectonophysics 298: 103-132.

Goussev SA, Charters RA, Peirce JW, Glenn WE (2003). Jackpine magnetic anomaly: Identification of a buried meteorite impact structure. The Leading Edge 22: 740-741.

Goussev SA, Griffith L, Peirce J, Cordsen A (2004). Enhanced HRAM anomalies correlate faults between 2D seismic lines. In: 74th Annual International Meeting, SEG, Extended Abstracts, p. 730.

Innocenti F, Mazuoli R, Pasquare G, Radicati F, Villan L (1982). Anatolia and north-western Iran. Thorpe, ed., Andesites. John Wiley and Sons.

Kalyoncuoglu UY, Anadolu NC, Baykul A, Erek Y (2010). Isparta şehir merkezi yüzey toprağındaki radyoaktivite düzeyi. Süleyman Demirel University Journal of Natural and Applied Sciences 14 (1): 111-119 (in Turkish).

Kanasewich ER, Agarwal RG (1970). Analysis of combined gravity and magnetic fields in wave number domain. Journal of Geophysical Research 75: 5702-5712.

Karaman ME (1990). Geological features of South Isparta. Geological Bulletin of Turkey 33: 57-67 (in Turkish).

Kunaratram K (1981). Simplified expressions for the magnetic anomalies due to vertical rectangular prisms. Geophysical Prospecting 29: 883-890. doi: 10.1111/j.1365-2478.1981.tb01032.x

Langenheim VE, Jachens RC, Morton DM, Kistler RW, Matti JC (2004). Geophysical and isotopic mapping of preexisting crustal structures that influenced the location and development of the San Jacinto fault zone, southern California. Geological Society of America Bulletin 116: 1143-1157.

Marquardt D (1963). An algorithm for least-squares estimation of nonlinear parameters. SIAM Journal on Applied Mathematics 11: 431-441. doi: 10.1137/0111030

Moeck IS (2014). Catalog of geothermal play types based on geologic controls. Renewable and Sustainable Energy Reviews 37: 867-882. doi: 10.1016/j.rser.2014.05.032

Nabighian MN (1972). The analytic signal of two-dimensional magnetic bodies with polygonal cross-section: Its properties and used for automated anomaly interpretation. Geophysics 37: 507-517.

Nabighian MN, Grauch VJS, Hansen RO, LaFehr TR, Li Y et al. (2005). The historical development of the magnetic method in exploration. Geophysics 70 (6): 33-61.

Platevoet B, Elitok Ö, Guillou H, Bardintzeff JM, Yagmurlu F et al. (2014). Petrology of Quaternary volcanic rocks and related plutonic xenoliths from Gölcük volcano, Isparta Angle, Turkey. Origin and evolution of the high-K alkaline series. Journal of Asian Earth Sciences 92: 53-76. doi: 10.1016/j.jseaes.2014.06.012.

Platevoet B, Scaillet S, Guillou H, Blamart D, Nomade S et al. (2008). Pleistocene eruptive chronology of the Gölcük volcano, Isparta Angle, Turkey. Quaternaire 19 (2): 147-156.

Poisson A (1977). Recherches geologique dans les 'uuri-des occidentales These Doct. d'Etat Orsay, No: 1902.

Poisson A, Akay E, Dumont JF, Uysal Ş (1984). The Isparta angle. Geology of the Taurus belt. International Geology Symposium, pp. 11-16.

Power M, Belcourt G, Rockel E (2004). Geophysical methods for kimberlite exploration in northern Canada. The Leading Edge 23: 1124.

Rao DB, Babu NR (1993). A Fortran-77 Computer program for three-dimensional ınversion of magnetic anomalies resulting from multiple prismatic bodies. Computers and Geosciences 19: 781-801. doi: 10.1016/0098-3004(93)90050-F

Roest WR, Verhoef J, Pilkington M (1992). Magnetic interpretation using the 3-D analytic signal. Geophysics 55 (1): 116-125.

Sailhac P, Gibert D (2003). Identification of sources of potential fields with the continuous wavelet transform: two-dimensional wavelets and multipolar approximations. Journal of Geophysical Research 108 (B5): 2262. doi: 10.1029/2002JB002021

Salem A, Ravat D, Smith R, Ushijima K (2005). Interpretation of magnetic data using an enhanced local wavenumber (ELW) method. Geophysics 70 (2): 7-12.

Salem A, Williams S, Fairhead D, Smith R, Ravat D (2008). Interpretation of magnetic data using tilt-angle derivatives. Geophysics 73: 1-10.

Smith RP, Grauch VJS, Blackwell DD (2002). Preliminary results of a high-resolution aeromagnetic survey to identify buried faults at Dixie Valley, Nevada. Geothermal Resources Council Transactions 26: 543-546.

Smith DV, Pratt D (2003). Advanced processing and interpretation of the high resolution aeromagnetic survey data over the Central Edwards Aquifer, Texas. In: Proceedings from the Symposium on the Application of Geophysics to Engineering and Environmental Problems, Environmental and Engineering Society.

Spector A, Grant FS (1970). Statistical models for interpreting aeromagnetic data. Geophysics 35: 293-302.

Timur E (2009). Joint inversion of magnetic and electromagnetic data. PhD Thesis, Dokuz Eylül University, İzmir, Turkey (in Turkish).

Timur E (2014). Magnetic susceptibility and VLF-R investigations for determining geothermal blowout contaminated area: a case study from Alaşehir (Manisa/Turkey). Environmental Earth Sciences 72 (7): 2497-2510.

Timur E (2017). Assessment of vertical magnetic gradient data of Tuzla Fault using boundary analysis and 3-D ınversion techniques. Journal of Power and Energy Engineering 5: 33-45. doi: 10.4236/jpee.2017.512006

Thompson, DJ (1982). Spectrum estimation and harmonic analysis. Proceedings of the IEEE 70 (9): 1055-1096.

Tsokas GN, Papazachos, CB (1992). Two-dimensional inversion filters in magnetic prospecting: Application to the exploration for buried antiquities. Geophysics 57: 1004-1013.

Utsugi M (2019). 3-D inversion of magnetic data based on the L1–L2 norm regularization. Earth, Planets and Space 71: 73. doi: 10.1186/s40623-019-1052-4

Venkata Raju DC (2003). LIMAT: a computer program for least-squares inversion of magnetic anomalies over long tabular bodies. Computers and Geosciences 29: 91-98.

Wang J, Meng X, Li F (2015) A computationally efficient scheme for the inversion of large-scale potential field data, application to synthetic and real data. Computer and Geosciences 85: 102-111.

Wanyin W, Yu P, Zhiyun Q (2009). A new edge recognition technology based on the normalized vertical derivative of the total horizontal derivative for potential field data. Applied Geophysics 6: 226-233.

Waldron JW (1982). Structural history of the Isparta angle, SW Turkey, Evolution of Eastern Mediterranean. In: International Meeting Geological Society of London; Edinburgh, Scotland. Abs.-I, p. 11.

Wijns C, Perez C, Kowalczyk P (2005). Theta map: edge detection in magnetic data. Geophysics 70 (4): 39-43.

Yagmurlu F, Savaşçın Y, Ergün M (1997). Relation of alkaline volcanism and active tectonism within the evolution of the Isparta Angle, SW Turkey. The Journal of Geology 15: 717-728.

Yalçınkaya S, Ergin A, Afşar ÖP, Taner K (1986). Geology of Western Torides, Isparta Project Report. Ankara, Turkey: General Directorate of Mineral Research and Exploration (MTA) (in Turkish).

Yalçınlar İ (1968). Structural Geomorphology. Vol. I. İstanbul University, Pub. No: 878. 2nd ed. İstanbul, Turkey: İstanbul University, p. 943 (in Turkish).